HHS Public Access

Author manuscript

J Biophotonics. Author manuscript; available in PMC 2019 August 10.

Published in final edited form as:

J Biophotonics. 2019 August ; 12(8): e201900066. doi:10.1002/jbio.201900066.

Wearable optical resolution photoacoustic microscopy

Qian Chen[1,2], **Huikai Xie**[3], **Lei Xi**[1,*]

[1]Department of Biomedical Engineering, Southern University of Science and Technology, Shenzhen, Guangdong, China

[2]School of Electronic Science and Engineering, University of Electronic Science and Technology of China, Chengdu, Sichuan, China

[3]Department of Electrical and Computer Engineering, University of Florida, Gainesville, Florida

Abstract

Optical resolution photoacoustic microscopy (ORPAM) is an emerging imaging technique, which has been extensively used to study various brain activities and disorders of the anesthetized/restricted rodents with a special focus on the morphological and functional visualization of cerebral cortex. However, it is challenging to develop a wearable photoacoustic microscope, which enables the investigation of brain activities/disorders on freely moving rodents. Here, we report a wearable and robust optical resolution photoacoustic microscope (W-ORPAM), which utilizes a small, light, stable and fast optical scanner. This wearable imaging probe features high spatiotemporal resolution, large field of view (FOV) and easy assembly as well as adjustable optical focus during the in vivo experiment, which makes it accessible to image cerebral cortex activities of freely moving rodents. To demonstrate the advantages of this technique, we used W-ORPAM to monitor both morphological and functional variations of vasculature in cerebral cortex during the induction of ischemia and reperfusion of a freely moving rat.

Graphical Abstract

[*]**Correspondence** Lei Xi, Department of Biomedical Engineering, Southern University of Science and Technology, Shenzhen, Guangdong, 518055, China., xilei@sustc.edu.cn.

AUTHOR CONTRIBUTIONS

L.X. conceived the concept, proposed the experimental plans, supported and supervised the project. H.K.X. provided the MEMS scanner. Q.C. built the system, finished the experiments and prepared the manuscript.

SUPPORTING INFORMATION

Additional supporting information may be found online in the Supporting Information section at the end of this article.

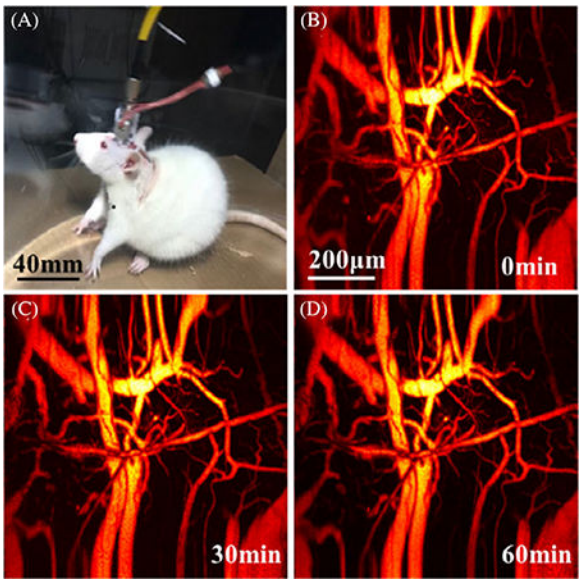

1 | INTRODUCTION

Understanding the complicated cerebral hemodynamics of rodents is a concerned issue in the communities of imaging, neuroscience, physiology and psychology [1, 2]. Recently, various optical imaging techniques, such as epifluorescence imaging, multi-photon microscopy, laser speckle and intrinsic optical imaging, have been developed to investigate neurovascular relationships in freely moving animals [3–6]. However, most of them suffer from inherent limitations such as small field of view (FOV), insufficient penetration depth and requirement of external contrast agent. Apart from optical imaging, functional ultrasound imaging is able to observe brain activities in freely moving rats with an ultrahigh temporal resolution [7]. Unfortunately, the spatial resolution is not capable of capturing microscopic neurovascular events and image contrast is low.

Optical resolution photoacoustic microscopy (ORPAM), featuring high spatial resolution, deep penetration depth and large FOV, is a noninvasive and label-free imaging approach capable of monitoring brain hemodynamics at microscale level [8–12]. Current developments of ORPAM mainly focus on miniaturization of the device using new scanning mechanisms and optical/acoustic scanners [8, 13–17]. However, it is challenging to develop a wearable photoacoustic microscope, which enables the investigation of brain activities on a freely moving rodent. There are two major challenges: (a) the lack of a small, light, stable and fast optical scanner, which is applicable for ORPAM; (b) optimal design of the miniaturized photoacoustic microscope, which owns high image quality and is easy to assemble, optimize and adjust during the in vivo experiment. Hu group proposed a conventional motorized-scanner-based photoacoustic microscope to image cerebral hemodynamics in awake mice restricted by an angle- and height-adjustable head-restraint apparatus [18]. Xi et al. developed a miniature hybrid probe integrating photoacoustic sensor and microelectrodes to study brain hemodynamics of freely moving rats [19]. However, this technique is invasive and only able to visualize hemodynamics in one spatial point.

Utilization of an electrical-micro-mechanical-system (MEMS) based optical scanner, we reported an ultracompact photoacoustic microscope with a size of 22 × 30 × 13 mm^3 and a weight of 20 g, which was still not appropriate for freely moving rodents [20–22].

In this study, we proposed and developed a wearable and robust optical resolution photoacoustic microscope, which utilizes a small, light, stable and fast optical scanner. We monitored the cerebral hemodynamics of freely moving rats, showing a long-term stability of the imaging probe. Thereafter, we established an ischemia and reperfusion model to investigate and quantify the evoked hemodynamic response of cerebral cortex under different physiological conditions.

2 | MATERIALS AND METHODS

2.1 | Animal preparation

Female Sprague-Dawley rats (n = 12), weighting 200 to 250 g, were used. The ethic committee at the Southern University of Science and Technology (SUSTech) has approved all the experimental procedures. After the experiments, all the rats were sacrificed following a standard procedure approved by SUSTech.

2.2 | Surgery and experiments

In order to evaluate the stability of W-ORPAM, we continually imaged cerebral cortex of a freely moving rat for 2 hours. Before the experiment, the rats were anesthetized by intraperitoneal injection of chloral hydrate at a dose of 50 mg/kg. A feedback-controlled heating pad was used to maintain the body temperature at 37.0 ± 0.5°C during the surgery. Then, we did craniotomy to remove both the scalp and skull over a circular area with a diameter of 7 mm in the left hemisphere. The dura was kept intact and continually bathed with artificial cerebrospinal fluid. Post the surgery, we attached an adaptor on the skull and fixed it with screws. The imaging probe was mounted on the adaptor and immobilized with both screws and hot glue. We optimized the imaging quality through adjusting the effective focal length of the collimator.

After the evaluation of the systemic stability, we carried out the in vivo study of cerebral hemodynamics during the conditions of ischemia and reperfusion. To establish the ischemia model, we anesthetized the rat, then permanently ligated two vertebral arteries inside the nape using electrical coagulation and sutured the surgical wound. The rat was kept in the cage with supply of water for 24 hours. Post the fully recovery of the rat from the first surgery, we separated bilateral carotids, did the craniotomy on the brain and mounted the imaging probe. After the optimization of the image quality, we monitored the normal cerebral hemodynamics for 5 minutes as the baseline. Then, we randomly divided 10 rats into two groups and performed two types of ischemia/reperfusion by ligating the bilateral carotids for 10 and 20 minutes, respectively.

2.3 | The imaging system

Figure 1A presents the schematic of the system. A 532 nm laser beam emitted from a high-repetition-rate (up to 600 kHz) pulsed laser (GLPM-10, IPG Photonics) with a duration of

1.7 nanoseconds is filtered by a customized spatial filter, which consists of two objectives and a 15-μm pinhole. The filtered laser beam is then coupled into an optical rotary joint (MJP-532–46-FC, Princetel Inc.) using a space- to-fiber coupler that is integrated with a customized electrical slip ring to allow the free movement of the rat. A multifunctional data acquisition card (PCI-6733, National Instrument) is used to generate four triangle waveforms with a peak-to-peak voltage of 5 V to drive the movement of the MEMS scanner via the conductive slip ring. The induced photoacoustic signals are detected by a customized flat transducer (center frequency: 10 MHz, bandwidth: 80%), amplified by a homemade ~66 dB preamplifier, filtered by a band-pass filter (5–20 MHz) to remove electromagnetic noise, and digitized using a fast data acquisition card (ATS-9325, Alazar Inc.) at a sampling rate of 100 MS/s. Figure 1B shows the enlarged view of the image probe. The output laser beam from the optical rotary joint is collimated using an adjustable optical collimator (CFC-5X-A, Thorlabs Inc.), then reflected by a right-angle prism (MRAP1–4.0, MT Optics). We use a plano-convex lens (LA 1222-A, Thorlabs Inc.) with a numerical aperture value of 0.2 to focus the laser beam, and a MEMS scanner (WM-L5–5, Wiotek) with a mirror size of 2 mm in diameter to carry out two-dimensional raster scanning of the converging laser beam. A water cube with a ultrathin cover glass tilted with an angle of 45° serves as the optical/acoustic combiner, which allows the fully transmission of light and partial reflection of acoustic waves. The imaging probe weights 8 g, which is appropriate for rats. It costs 10 seconds to cover a rectangle FOV of 1.2 mm × 1.2 mm. As shown in Figure 1C,D, the systemic lateral and axial resolutions are measured as 2.25 and 105 μm, respectively, based on phantom experiments. The lateral resolution deterioration is caused by both the curvature of the MEMS scanner and the mismatches of the reflective indices among air, glass and water in the light path. The laser energy per pulse that reaches the surface of brain is under 100 nJ, which will not lead to tissue damage for in vivo animal experiments [20].

2.4 | Image reconstruction and processing

All raw photoacoustic signals were first processed with Hilbert transform and then directly back-projected to a rectangular coordinate. We show all volumetric data by projecting the maximal amplitude of each A-line and obtain the maximum amplitude projection (MAP) image captured from different time points.

MATLAB (R2012 b, MathWorks) was used for post-processing of MAP images. We enhanced the contrast of blood vessels by using an adaptive histogram equalization (AHE) algorithm, sharped the edge of blood vessels via a high pass filter, and improved the signal-to-noise ratio (SNR) by applying Gabor wavelet transformation, Top hat operators and Hessian matrix. We calculated and normalized the total hemoglobin and total vascular numbers. We carried out the statistical analysis by using mean ± SD in the graphic display in Figure 4C,D.

3 | RESULTS

Figure 2A presents the in vivo imaging of the cerebral cortex at 0, 30, 60 and 90 minutes post the fully recovery of the rat, respectively. Figure 2B shows the photograph of a freely moving rat wearing the imaging probe in the tank. Video S1 shows that the rat freely moves

in a transparent tank (left) and longitudinal recording of cerebral hemodynamics with an imaging interval of 10 seconds over 2 hours (right). During the entire course of the experiment, the imaging quality keeps stable with no obvious deterioration of contrast, FOV and spatial resolution. We randomly selected 100 MAP images and calculated the fluctuation of photoacoustic intensity. Figure 2C presents the derived fractional changes, which are less than 5% possibly due to the complicated physiological changes during the experiments.

Figure 3 shows the MAP images of two groups with different types of ligation and reperfusion. The first row presents the MAP images prior to the operation, which serve as the baseline. The second, third and fourth rows show the MAP images post the first, second and third ligations and reperfusions. Based on the images, we observe that the photoacoustic intensity, which represents the relative concentration of total hemoglobin, over the entire FOV suddenly decrease post the ligation in both groups, and the photoacoustic intensity can rapidly recover post the perfusion from the carotid. We are noticed that the fractional changes in the second group post the second and third ligation are much weaker than that of the first ligation. Besides the concentration of total hemoglobin, some of the blood vessels start to shrink immediately post the ligation as indicated by the white arrows in both groups. Video S2 presents the behavior of the rat and operations of ligation and reperfusion, in which we find that the rat partially loses the balance and functions of limbs. Videos S3 and S4 show typical hemodynamic changes during the entire course of experiments in two groups.

Figure 4A,B shows the quantitative analysis of total hemoglobin and diameters of the selected vessels marked by white lines (Figure 3A,B), and the relative concentration of total hemoglobin as well as the total number of blood vessels over the entire FOV. Figure 4A shows that both the total hemoglobin inside a single blood vessel and the concentration of total hemoglobin over the entire imaging domain decrease significantly post the operation of carotid ligation and partially recover after the reperfusion, which is consistent with the visible changes in images. In addition, the rats in the second group (Figure 4B) cannot recover after the first ligation, which might be caused by the long-term lack of blood supply and potential embolism. Similar to the hemodynamics, the size of a selected blood vessel and the vascular number over the FOV have the same tendency. As shown in Figure 4C,D, we carried out statistical analysis of the relative concentration of total hemoglobin and the total number of blood vessels over the entire FOV. The results show that most of rats have the similar responses to the ischemia and perfusion in both groups.

4 | DISCUSSION

Optical resolution photoacoustic microscopy allows detection of both structural and functional information of cerebral vascular network with rich contrast and a cellular resolution. However, no existing ORPAMs can be applied for the study of freely moving rodents. In this study, the proposed a wearable optical resolution photoacoustic microscope, which owns the features of miniature, light, high-speed volumetric imaging capability, high spatial resolution and long-term stability for brain investigations of freely moving rodents. However, to carry out the investigation of complicated brain activities/disorders and broad

the impact of this technique, further improvement should be considered. First, to derive more functional parameters such as oxygen saturation and blood flow, multispectral strategy using more than two wavelengths and employment of photoacoustic Doppler Effect are required. Second, to investigate chronic brain diseases such as tumor, spontaneous seizures, Alzheimer disease, a longterm optical/ultrasonic transparent window is preferred. Third, we need to introduce imaging/sensing techniques to simultaneously study neural activities and hemodynamics of the brain, and uncover the neurovascular relationships.

Supplementary Material

Refer to Web version on PubMed Central for supplementary material.

ACKNOWLEDGMENTS

This work was sponsored by National Natural Science Foundation of China (61775028, 81571722 and 61528401); Startup grant from Southern University of Science and Technology; National Key Research and Development Program (2017YFC0108300); National Institutes of Health (R01EB020601).

Funding information

Southern University of Science and Technology; National Natural Science Foundation of China, Grant/Award Numbers: 81571722, 61775028, 61528401

Biography

Qian Chen is currently a first-year doctoral student. Now, she is working as a visiting student in the Multi-Functional Optical Imaging Lab (MFOIL) at the Southern University of Science and Technology, Shenzhen, China. Her research focuses on developing novel handheld and wearable optical resolution photoacoustic microscopy systems for biological and clinical research.

Huikai Xie is a full professor in the Department of Electrical and Computer Engineering at the University of Florida. His current research focuses on developing innovative integrated microsystems using micro/nanofabrication techniques for medical, industrial, space and consumer electronics applications.

Lei Xi received his bachelor degree from Huazhong University of Science and Technology, Wuhan, China (2007) in optics, and finished his doctoral and post-doctoral training in the Department of Biomedical Engineering at the University of Florida, Gainesville, USA, in 2012 and 2014, respectively. Then, he moved to the University of Electronic Science and Technology of China (UESTC) at the end of 2014 as a professor. From 2018, he joined the Department of Biomedical Engineering at the Southern University of Science and Technology (SUSTech). He is hosting the multifunctional optical imaging lab (MFOIL) in SUSTech and focusing on developing novel optical imaging techniques for different biomedical and clinical studies.

REFERENCES

[1]. Silaisi G, Xiao DS, Vanni MP, Chen ACN, Murphy TH, J. Neurosci. Methods 2016, 267, 141. [PubMed: 27102043]

[2]. Thom PS, Calvin JK, Daryl KB, David CI, Sang HC, Afonso CS, J. Neurosci. Methods 2016, 271, 55. [PubMed: 27393311]

[3]. Sawinski J, Wallace DJ, Greenberg DS, Grossmann S, Denk W, Kerr JND, Proc. Natl. Acad. Sci. USA 2009, 106, 19557. [PubMed: 19889973]

[4]. Lee AK, Manns LD, Sakmann B, Brecht M, Neuron 2006, 51, 399. [PubMed: 16908406]

[5]. Miao P, Tong SB, Liu HY, Liu Q, Li Y, J. Biophotonics 2011,16, 090502.

[6]. Ferezou I, Bolea S, Petersen CC, Neuron 2006, 50, 617. [PubMed: 16701211]

[7]. Urban A, Dussaux C, Martel G, Brunner C, Mace E, Montaldo G, Nat. Methods 2015, 12, 873. [PubMed: 26192084]

[8]. Yao JJ, Wang LD, Yang JM, Maslov k. I., Wong TTW, Li L, Huang CH, Zhou J, Wang LV, Nat. Methods 2015, 12, 407. [PubMed: 25822799]

[9]. Reblin J, Estrada H, Gottachalk S, Sela G, Zwack M, Wissmeyer G, Ntziachristos V, Razansky D, J. Biophotonics 201811, e201800057 10.1002/jbio.201800057. [PubMed: 29675962]

[10]. Bi R, Balasundaram G, Jeon S, Tay HC, Pu Y, Li XT, Moothanchery M, Kim C, Olivo M, J Biophotonics 2018, 11, e201700327 10.1002/jbio.201700327. [PubMed: 29419946]

[11]. Yang SH, Xing D, Zhou Q, Xiang LZ, Lao YQ, Med. Phys 2007, 34, 3294. [PubMed: 17879793]

[12]. Yang HSH, Xing D, Lao YQ, Yang DW, Zeng LM, Xiang LZ, Chen WR, Appl. Phys. Lett 2007, 90, 243902.

[13]. Lin L, Zhang P, Xu S, Shi J, Li L, Yao J, Wang L, Zhou J, Wang LV, J. Biomed. Opt 2017, 4, 41002.

[14]. Kim JY, Lee C, Park K, Lim G, Kim C, Sci. Rep 2015, 5, 7932. [PubMed: 25604654]

[15]. Qi WZ, Chen Q, Guo H, Xie HK, Xi L, Micromachines 2018, 9, 288.

[16]. Qin W, Chen Q, Xi L, Biomed. Opt. Express 2018, 9, 2205. [PubMed: 29760981]

[17]. Guo H, Song CL, Xie HK, Xi L, Opt. Lett 2017, 42, 4615. [PubMed: 29140326]

[18]. Cao R, Li J, Ning B, Sun ND, Wang TX, Zuo ZY, Hu S, Neuroimage 2017, 150, 77. [PubMed: 28111187]

[19]. Xi L, Jin T, Zhou JL, Carney P, Jiang HB, Neuroimage 2017,161, 232. [PubMed: 28818693]

[20]. Chen Q, Guo H, Jin T, Qi WZ, Xie HK, Xi L, Opt. Lett 2018, 43, 1615. [PubMed: 29601044]

[21]. Guo H, Chen Q, Qi WZ, Chen XX, Xi L, J. Biophotonics 201811, e201800067 10.1002/jbio.201800067. [PubMed: 29671952]

[22]. Chen Q, Guo H, Qi WZ, Gan Q, Yang L, Ke BW, Chen XX, Jin T, Xi L, J. Biophotonics 2018, 12, e201800348 10.1002/jbio.201800348. [PubMed: 30421586]

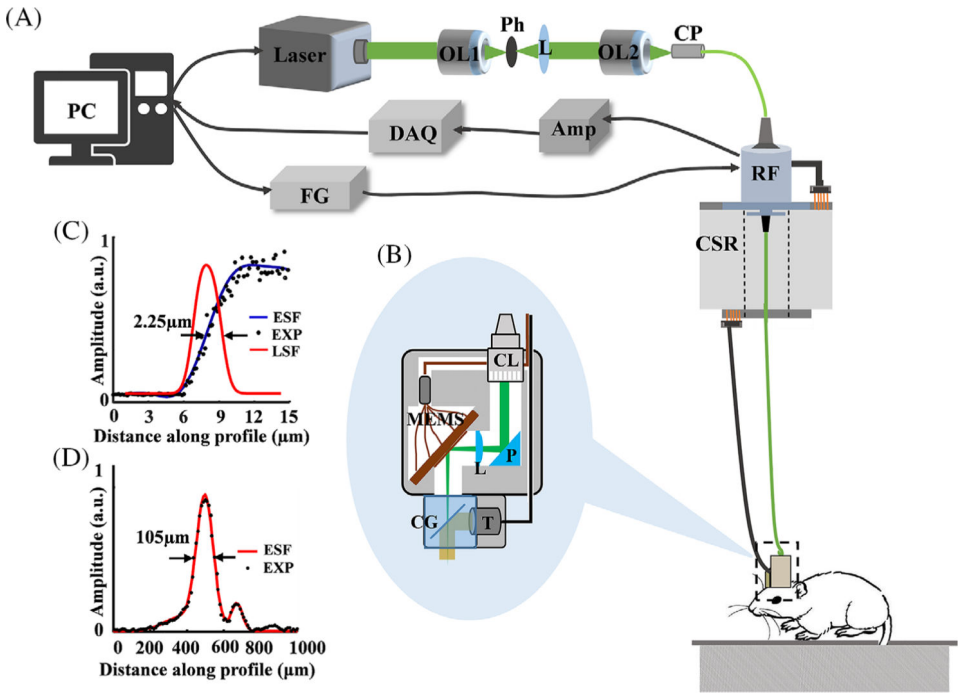

FIGURE 1.

System configurations and performance evaluation. A, The schematic of the system. B, An enlarged view of the imaging probe. C, Experimental estimation of the lateral resolution. D, Experimental estimation of the axial resolution. PC, personal computer; OL1-OL2, objective; Ph, pinhole; L, convex lens; CP, coupler; DAQ, data acquisition card; Amp, amplifier; FG, functional generator; RF, optical rotary joint; CSR, conductive slip ring; CL, optical collimator; P, right angle prism; L, focus lens, MEMS, mechanical and electrical system mirror; CG, cover glass; T, transducer

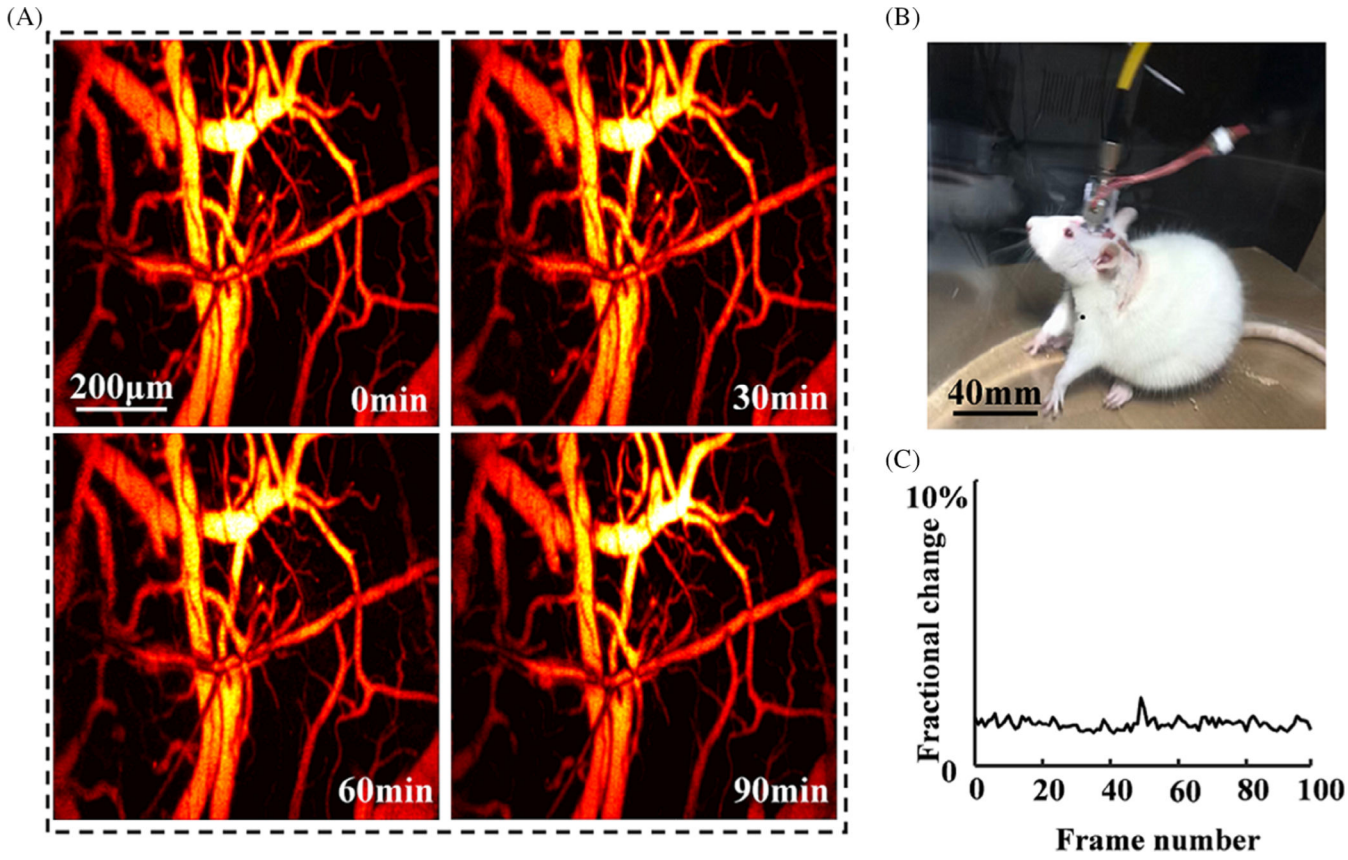

FIGURE 2.

Evaluation of stability and robust of the imaging probe. A, Four typical images captured at 0, 30, 60 and 90 minutes, respectively. B, A photograph of a rat wearing the imaging probe. C, The fractional change of photoacoustic intensity

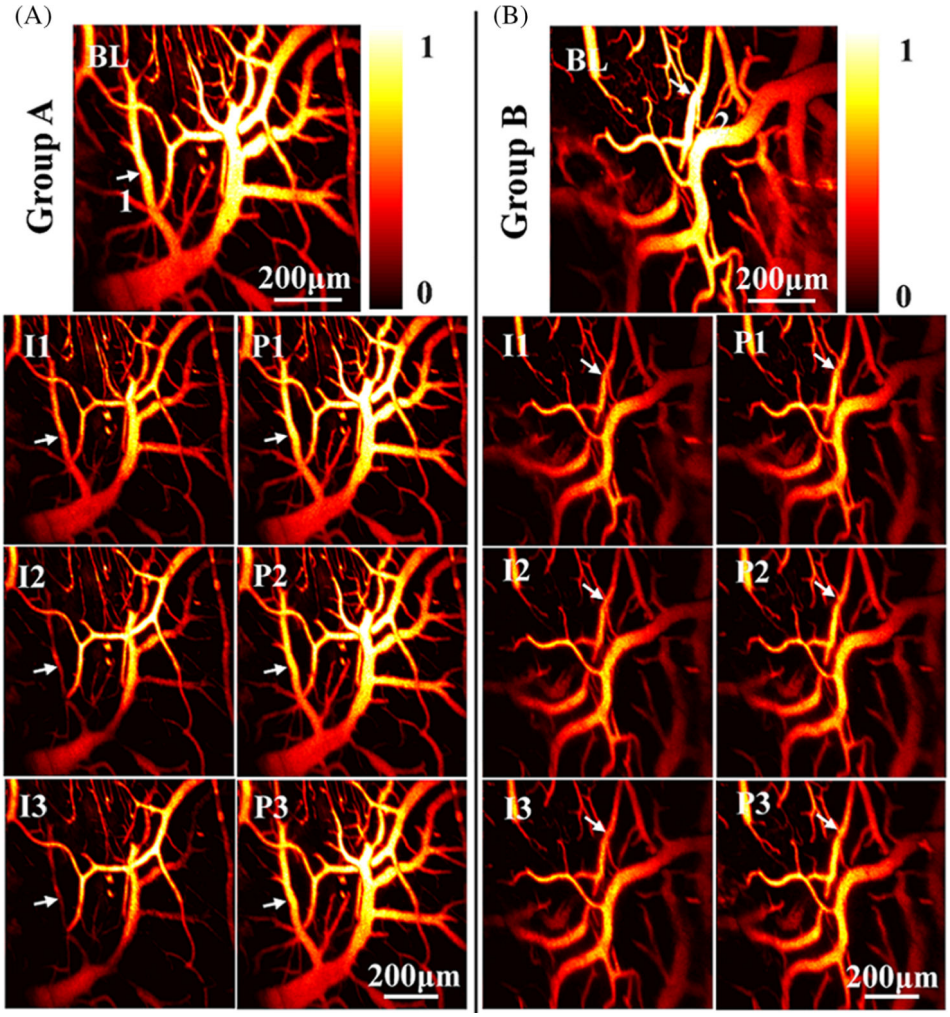

FIGURE 3.

Photoacoustic visualization of cerebral hemodynamics during ischemia and reperfusion. A, The first row shows the MAP image of a typical rat brain before bilateral carotid ligation in the first group. I1 and P1 present the MAP images post the first 10-minute ligation and reperfusion. I2 and P2 present the MAP images post the second 10-minute ligation and reperfusion. I3 and P3 present the MAP images post the third ligation and reperfusion. B, Representative MAP images of the second group with a different ligation/reperfusion time of 20 minutes

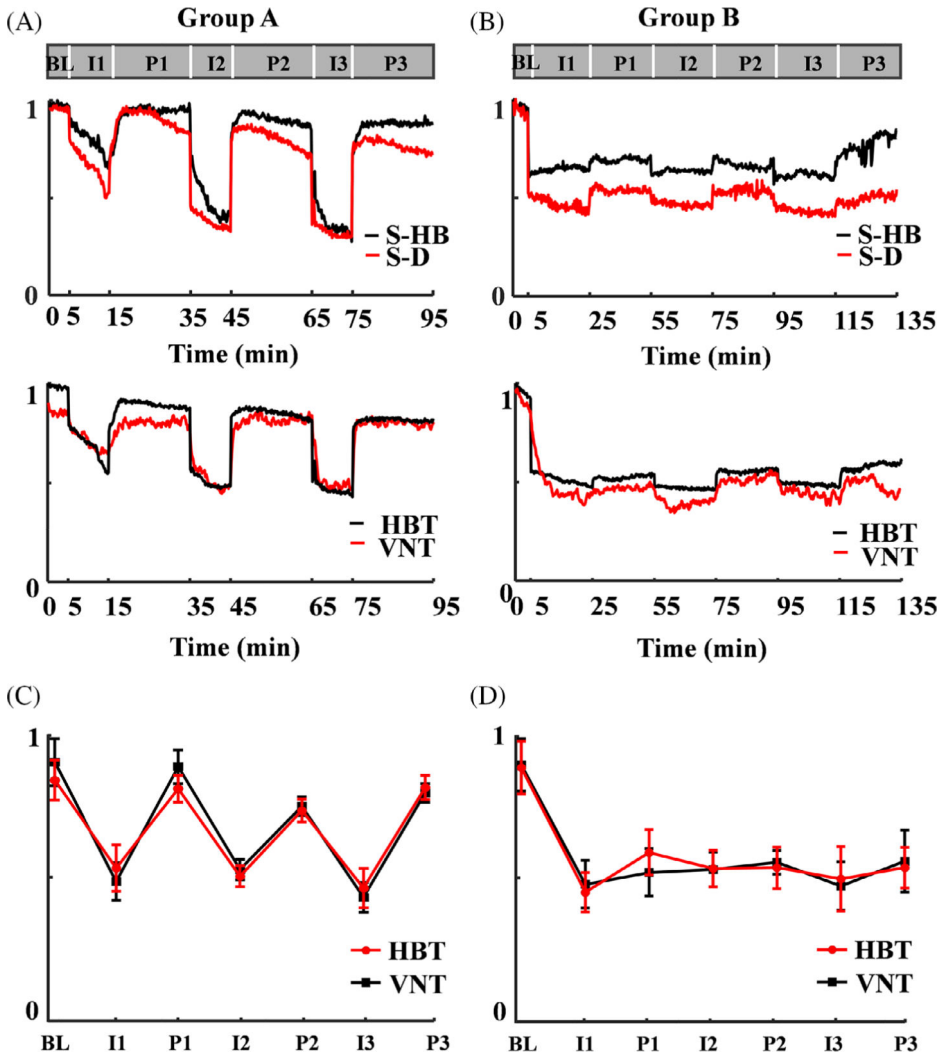

FIGURE 4.

Quantitative analysis of total hemoglobin inside selected vessels, diameters of selected vessels, total hemoglobin in the image domain and total vascular numbers over the entire FOV in Group A (A) and Group B (B). The statistical analysis of total hemoglobin and total vascular numbers in each stage in group A (C) and group B (D). S-HB, total hemoglobin in selected vessels; S-D, diameters of selected vessels; HBT: total hemoglobin; VNT, total vascular number. BL: Baseline, I1: the first time to ligation, P1: the first tome to perfusion, I2: the second time to ligation, P2: the second time to perfusion; I3: the third time to ligation, P3: the third time to perfusion, error bar means the mean ± SD